JAAS

Accepted Manuscript

This article can be cited before page numbers have been issued, to do this please use: J. Jiménez-Lamana, I. Abad-Álvaro, B. Katarzyna, F. Laborda, J. Szpunar and R. Lobinski, *J. Anal. At. Spectrom.*, 2018, DOI: 10.1039/C7JA00378A.

View Article Online
DOI: 10.1039/C7JA00378A

Detection and characterization of biogenic selenium nanoparticles in selenium-rich yeast by single particle ICPMS

Javier Jiménez-Lamana [a,*], Isabel Abad-Álvaro [b], Katarzyna Bierla [a], Francisco Laborda [b], Joanna Szpunar [a], Ryszard Lobinski [a]

[a]Laboratoire de Chimie Analytique Bio-inorganique et Environnement (LCABIE), UMR 5254-IPREM, CNRS-UPPA, Hélioparc, Pau, France

[b]Group of Analytical Spectroscopy and Sensors (GEAS), Institute of Environmental Sciences, (IUCA) University of Zaragoza, Zaragoza, Spain

Corresponding author

*Telephone: +33540175037. E-mail: j.jimenez-lamana@univ-pau.fr

ABSTRACT

A method based on single particle inductively coupled plasma mass spectrometry (SP-ICPMS) was developed for the analysis of commercial Se-rich yeasts, to confirm the occurrence of selenium nanoparticles in these food supplements. A considerable reduction of the background levels was achieved by combining data acquisition at microsecond dwell times and the use of H_2 reaction cell, improving by a factor of 10 the current state-of-the-art methodology, and bringing size detection

View Article Online
DOI: 10.1039/C7JA00378A

limits down to 18 nm for selenium nanoparticles. The presence of nanoparticulate selenium was unveiled by size-exclusion chromatography ICPMS, detecting a selenium peak at the exclusion volume of the column showing absorption at the wavelength corresponding to selenium nanoparticles. SP-ICPMS allowed to confirm the presence of Se-nanoparticles, as well as to calculate the nanoparticle size distribution, owing to the information about the shape and elemental composition of the nanoparticles obtained by transmission electron microscopy (TEM) and energy dispersive X-ray spectroscopy (EDS), respectively. These results reveal the significance of nanoparticles in the speciation of metals and metalloids in biological samples and the capability of SP-ICPMS in combination with TEM-EDS to carry out these analyses.

1. Introduction

Tailored metal/metalloid biogenic nanoparticles with specific physiochemical properties have been shown to be highly toxic to several pathogenic bacteria and may offer an attractive alternative for therapy of infections by antibiotic resistant bacteria.[1,2] In particular, selenium nanoparticles (SeNPs) synthesized by microorganisms, such as bacteria, fungi or yeast were demonstrated to possess antibacterial, antiviral and antioxidant properties.[1,2] The process of the Se° nanoparticle formation is based on the reduction of a toxic selenite (SeO_3^{2-}) or selenate (SeO_4^{2-}) to the less toxic (for the host organism) elemental selenium through the intra- or extracellular formation of SeNPs with a typical spherical shape and a diameter of 50-400 nm.[3,4]

Yeast is not only recognised as a model system to study selenite or selenate metabolic detoxification pathways,[5] but it has also been the basis of an important biotechnological process of their conversion to selenoamino acids, in particular to selenomethionine.[6] Indeed, yeast

View Article Online
DOI: 10.1039/C7JA00378A

(*Saccharomyces cerevisiae*) grown on selenite or selenate media, accumulates up to 3000 μg g^{-1} of selenium, and has been used as a food and feed supplement,[6] and at high doses (>200 μg Se/day) in prostate and colon cancer prevention treatments.[7] The subsequent authorizations obtained by several companies for the commercialization of Se-rich yeast were preceded by the development of analytical methods for the specific identification and quantification of the different chemical forms of selenium present (speciation) of which the state-of-the art was reviewed.[8]

The currently available analytical methods allow the determination of selenomethionine [with a relatively high confidence owing to the availability of a certified reference material (SELM-1)],[9] selenocysteine and a water soluble metabolome fraction.[8] They also allow the determination of the residual (non-reacted) selenite or selenate, referred to as "inorganic selenium" of which the presence below 2% is considered by the legislators as a proof of an "organic" character of Se-rich yeast.[10] Our experience over the past decade, through the analysis of several hundred samples from about 20 different suppliers, indicates that the selenium mass balance for the identified species rarely exceeds 90% which would suggest the presence of unaccounted forms of selenium.

To our best knowledge, Se° has never been quantified in yeast, although there were some attempts to its quantification in garlic[11] and in *Thunbergia alata*[12] using operationally defined or chemical conversion methods. Nanometer-sized deposits were reported in yeast cells grown in the presence of selenium by using X-ray radiation fluorescence spectroscopy[13] without being characterized more deeply or quantified. We are putting forward here a hypothesis that a certain amount of selenium may be present in Se-rich yeast supplements as SeNPs and are proposing the development of an analytical method for its verification.

View Article Online
DOI: 10.1039/C7JA00378A

To date SeNPs produced by microorganisms have been characterized by transmission electron microscopy (TEM),[3,4,14-19] X-Ray diffraction (XRD)[20] and atomic force microscopy (AFM).[19,20] For instance, TEM analyses provided evidence of the formation of electron-dense granules in Se-treated microorganisms which were absent in the control ones.[3,4] The presence of selenium in these granules could be confirmed by energy dispersive X-ray spectroscopy (EDS) while the absence of peaks from other elements indicated the presence of Se in the elemental state rather than as a selenide.[3,4] TEM was also applied for the characterization of SeNPs produced by *Bacillus cereus*,[14] the soil bacterium *Pseudomonas putida* KT2440,[15] the filamentous bacterium *Streptomyces sp.* ES2-5,[16] the rhizobacterium *Azospirillum brasilense,*[17,18] and a genetically modified *Pichia pastoris* strain.[19] In the latter case, results were confirmed by AFM. On the other hand, SeNPs of an average size of 21 nm produced by bacterial isolate *Pseudomonas aeruginosa* strain JS-11 were characterized by XRD.[20] The morphology and size of the nanoparticles were further validated by AFM. Recently, an alternative to TEM measurements was proposed by using the capabilities of asymmetrical flow field-flow fractionation (AF4) coupled on- and off-line with different detectors, such as diode array (DAD), dynamic light scattering (DLS) or inductively coupled plasma mass spectrometry (ICP-MS)[21,22]. For example, biogenic SeNPs synthesized by lactic acid bacteria (LAB) were characterized by AF4 coupled on-line with DLS and results in good agreement with those obtained by TEM and nanoparticle tracking analysis (NTA) were obtained[22]. A major drawback of these methods is their difficulty to detect, characterize and quantify SeNPs at low concentrations ($\mu g\ kg^{-1}$).

This limitation can be overcome by single particle inductively coupled plasma mass spectrometry (SP-ICPMS), which is one of the emerging techniques for the detection,

View Article Online
DOI: 10.1039/C7JA00378A

characterization and quantification of nanoparticles.[23] The theoretical basis of SP-ICPMS was outlined by Degueldre *et al*.[24] and further developed by Laborda *et al*.[25] SP-ICPMS is able to discriminate (detect and quantify) dissolved versus particulate forms of the element in a sample, and to provide information about the element mass content per particle. Moreover, if additional information about their composition, shape and density is available, the size of the particles can be obtained, as well as their number and mass concentration.[26]

The feasibility of SP-ICPMS is compromised by the achievable size detection limits. For elemental selenium nanoparticles, a detection limit of 200 nm was estimated theoretically.[27] This is by far too high for the microorganisms related applications, although this size detection limit was calculated by using the low abundant (9.36%) ^{76}Se isotope, due to inherent problems for selenium determination by ICPMS because of spectral interferences. This problem can usually be overcome by using mathematical correction equations[28] or reaction/collision cells[29].

The objective of this work is the development of a method for the detection and size characterization of selenium nanoparticles by single particle ICPMS with the aim to reduce considerably the size-detection limits predicted up to now.[27] The method is going to be used to verify the occurrence of inorganic nanoparticulate selenium in Se-rich yeasts, confirming the hypothesis that this species must be included in the speciation schemes of this element in Se-rich yeasts.

2. Experimental

2.1. Standards, samples and reagents

View Article Online
DOI: 10.1039/C7JA00378A

Diluted suspensions of gold and selenium nanoparticles were prepared from commercially available materials. A reference gold nanoparticle suspension RM 8013 of 60-nm nominal diameter was obtained from NIST (NIST, Gaithersburg, MD). Suspensions of selenium nanoparticles of nominal diameters of 50 and 100 nm were purchased from Nanocs (Nanocs, New York, NY). Dilutions were prepared in ultrapure water by accurately weighing (± 0.1 mg) aliquots of the stock suspensions after 1 min sonication (Branson 2510, Bransonic, Danbury, CT; nominal power and frequency: 100 W, 42 kHz +/- 6%). After dilution and before each analysis, the suspensions were bath sonicated for 1 min (same power and frequency). Longer sonication times were not used to avoid excessive heating of the suspensions. Aqueous selenium solutions were prepared from a standard stock solution of 10000 mg L^{-1} (Sigma-Aldrich, St. Louis, MO) by dilution in ultrapure water. Ultrapure water (18.2 MΩ cm) was obtained from a Milli-Q system (Millipore, Guyancourt, France). Selenium-rich Brewer's yeast samples (obtained from a commercial provider), corresponding to a yeast strain *Saccharomyces cerevisiae*, grown in different concentrations of selenium were used.

2.2. SP-ICPMS analysis and data processing

An Agilent 7900 Inductively Coupled Plasma Mass Spectrometer (ICPMS) (Agilent, Tokyo, Japan) was used throughout. The sample introduction system consisted of a concentric nebulizer and a quartz cyclonic spray chamber. Default instrumental and data acquisition parameters are listed in Table 1. Settling time during data acquisition was eliminated and the total acquisition time was 60 s in all experiments.

Nebulization efficiency was calculated according to the particle frequency method developed by Pace *et al*.[30] The sample flow rate was calculated daily by measuring the mass of

View Article Online
DOI: 10.1039/C7JA00378A

water taken up by the peristaltic pump for two minutes. This operation was repeated three times and the average value used for calculations. Under the experimental conditions used along this work, the nebulization efficiency at a sample flow rate of 0.35 mL min^{-1} was 3.5 %.

Dwell times of 5 ms and 100 µs were studied and isotopes ^{80}Se and ^{78}Se monitored. Single Nanoparticle Application Module for ICPMS MassHunter software (Agilent), as well as in-house developed programs based on MatLab (MathWorks, Natick, MA) and Excel (Microsoft, Redmond, OR) spreadsheets were used for data processing. OriginPro 8 data analysis software (OriginLab Corporation, Northampton, MA) was also used.

Table 1 Default instrumental and data acquisition parameters for single particle ICPMS

Instrumental parameters	
RF Power	1550 W
Argon gas flow rate	
Plasma	15 L min^{-1}
Auxiliary	0.9 L min^{-1}
Nebulizer	1.10 L min^{-1}
Reaction cell flow rate (H_2)	5.0 mL min^{-1}
Sample uptake rate	0.35 mL min^{-1}
Data acquisition parameters	
Dwell time	5 ms, 100 µs
Readings per replicate	12000, 600000
Settling time	-
Total acquisition time	60 s
Isotopes monitored	^{78}Se, ^{80}Se, ^{197}Au

View Article Online
DOI: 10.1039/C7JA00378A

2.3. Size Exclusion chromatography – ICPMS

A Superdex Peptide 10/300 GL column (GE Healthcare, Pittsburgh, PA) was coupled to an Agilent 7700x ICPMS (Agilent) instrument. Chromatographic separations were performed by using a model 1200 series HPLC pump (Agilent) as a delivery system. The exit of the column was connected in series to an UV-visible detector (Agilent) and the ICPMS instrument.

2.4. Transmission electron microscopy

Samples were prepared on holey carbon films on mesh copper grids. A few microliters of each sample were dropped on the grid and left to dry completely. Images were obtained using a FEI TECNAI 12 (FEI, Hillsboro, OR) and recorded using an ORIUS SC1000 11MPx (GATAN, Pleasanton, CA) CCD camera. The microscope is equipped with an energy-dispersive X-ray analysis system for elemental analysis.

2.5. Procedures

2.5.1. Acid digestion. The content of total selenium in selenium nanoparticle suspensions and Se-rich yeast samples was determined by ICPMS following acid digestion in a DigiPREP digestion system (SCP Science, Quebec, Canada). 250 µL of H_2O_2 (VWR International, Fontenay-sous-Bois, France) and 1 mL of conc. HNO_3 (Baker, Deventer, Netherlands) were added to 250 µL of sample. The digestion was performed at 65 °C for 4 h. After digestion the volume was made up to 50 mL so that the final HNO_3 concentration was 2% (v/v). Digestions were made in duplicate. Blanks were run in parallel with the samples, as well as Certified Reference Material SELM-1

View Article Online
DOI: 10.1039/C7JA00378A

(National Research Council of Canada) was analysed in order to validate the total selenium determination after acid digestion.

2.5.2. Enzymatic digestion. The digestion/extraction procedure included four steps: (1) 200 mg of a Se-rich yeast sample were suspended in 5 mL of water, bath sonicated for 1 h and centrifuged at 4500 x g for 10 min; (2) the pellet was resuspended with a solution of 5 mL of driselase (Sigma Aldrich, Saint-Quentin Fallavier, France) 4% (*m/v*) in Tris (Sigma Aldrich) 30 mM at pH 7.5, incubated at 25°C for 17 h and centrifuged at 4500 x g for 10 min; (3) the pellet was resuspended with a solution of 5 mL of protease (Sigma Aldrich) of 4 mg L^{-1} in Tris 30 mM at pH 7.5, incubated at 37°C for 17 h and centrifuged at 4500 x g for 10 min; (4) finally, the pellet was resuspended with a solution of 5 mL of sodium dodecyl sulphate (SDS, Sigma Aldrich) of 4% (*m/v*), bath sonicated for 1 h and centrifuged at 4500 x g for 10 min. The supernatant was recovered and kept at 4°C until analysis. One of the samples was subjected to an extra step: 1 mL of the SDS extract was digested with a 1 mL protease solution of 4 mg L^{-1} in Tris 30 mM at pH 7.5, incubated at 37°C for 17 h and centrifuged at 4500 x g for 10 min.

3. Results and discussion

3.1. Selection of instrumental parameters for the improvement of size detection limits

In SP-ICPMS, the size detection limit is critically dependent on the detection efficiency (ions arriving to the detector with respect to the atoms in the plasma) and the background signal. Isobaric and matrix/plasma polyatomic interferences, as well as dissolved species of the element measured contribute to the continuous baseline in the time scans recorded in single particle mode. The most

View Article Online
DOI: 10.1039/C7JA00378A

significant effect of a high baseline level is the loss of capability to identify particles with smaller amounts of the element measured, and hence the increase in the size detection limits.[31]

Selenium has 6 naturally occurring stable isotopes with abundances from 0.9 to 49.6% which are severely interfered mostly by Ar containing ions (Table S1). This problem has been overcome in quadrupole ICPMS by selecting less-interfered isotopes (e.g., ^{82}Se) or by using mathematical correction equations.[28] However, the use of reaction/collision cells[29] should allow the use of the most abundant isotopes ^{80}Se and ^{78}Se,[32,33] which are otherwise severely interfered by Ar dimers. The fact that the size detection limit value of 200 nm was estimated by Lee *et al*.[27] using relatively-low abundant ^{76}Se (9.36%) suggests a large margin for improvement of the size detection limit of SeNPs if a high abundance isotope is selected and the polyatomic interferences removed. Finally, a decrease of dwell times from milliseconds to microseconds would result in a proportional reduction of the absolute baseline level[34] and hence of the related noise. The above considerations were the basis of the method optimization strategy.

3.1.1. Choice of the isotope: effect of the collision cell. Our goal was to use one of the two most abundant selenium isotopes, ^{78}Se and ^{80}Se, by reducing or eliminating the background interferences. Apart from the contribution of residual Kr in the Ar gas supply, the main plasma background contributions at masses 78 and 80 arise from Ar dimers. Indeed, the direct measurement at m/z 80 is not possible, as the background exceeds 6.4 x 10^7 cps (time scans are shown in Fig. S1); a considerable background (4.1 x 10^4 cps) is also observed for ^{78}Se. The use of collision/reaction cells to reduce argon-based polyatomic interferences has been previously reported in literature (but never for selenium in the single-particle mode), with the use of different gases such as methane[35-37] or a He-H_2 mixture.[32] For instance, the potentially interfering argon dimers at the selenium masses

View Article Online
DOI: 10.1039/C7JA00378A

74, 76, 78 and 80 were reduced by approximately five orders of magnitude by using methane as reactive cell gas.[35] In our case, the pressurization of the collision cell with H_2 (5.00 mL min^{-1}) led to a 5 x 10^3-fold decrease in the background for ^{78}Se (down to 8 cps) and 7 x 10^5-fold for ^{80}Se (down to 90 cps). Therefore, the use of the reaction cell leads to an important decrease of background signals in both cases, being more pronounced at mass 80. If sensitivities at mass 78 with and without reaction cell are compared, an improvement of more than twice is observed using H_2, which is explained through the isotopic abundance of the isotopes. Table 2 summarizes the background signals, the standard deviation of the associated noise, the signal-to-noise ratio and the sensitivity (slope of the calibration curve for selenium water solution) which allowed the calculation of the attainable concentration detection limits for the different selenium isotopes in the standard and collision/reaction cell modes.

Table 2 Background signals, associated noise (expressed as standard deviation of background), signal-to-noise ratio, sensitivity and attainable concentration detection limits for the different selenium isotopes when measured with and without collision/reaction cell. Dwell time: 100 µs

Se	H_2 cell	Background (cps)	Noise (cps)	Sensitivity (cps L μg^{-1})	S/N	LD (µg L^{-1})
80	No	63700000	2160000	O/R	---	---
78	No	41300	18800	7700	0.04	7.33
80	Yes	90	995	40600	40.8	0.074
78	Yes	8	300	17800	59.33	0.051

3.1.2. Dwell time. When a sufficiently diluted suspension of nanoparticles is introduced into the plasma, each particle produces an individual pack of ions which is detected as such. By

View Article Online
DOI: 10.1039/C7JA00378A

using dwell times in the millisecond range (3-10 ms), events corresponding to the detection of single particles are detected as single pulses, whereas they are detected as transient signals when microsecond dwell times (<100-200 μs) are selected. On the other hand, the dissolved species present together with the residual plasma background, produce a constant signal in the detector. The intensity of this signal, expressed in counts, decreases proportionally if dwell times are shortened[32] whereas the corresponding noise diminishes according to the square root of the background (for signals below ca. 1000 counts, shot noise being the main contribution to the noise).[26]

Fig. 1 compares the time scans at dwell times of 5 ms and 100 μs with reaction cell recorded for water and for a 50-nm selenium nanoparticle suspension with a nanoparticle number concentration of ~ 1.85 x 10^8 L^{-1}. When working in the milliseconds regime (Figs. 1a, c), an averaged baseline signal of 3.4 counts was measured. However, when the dwell time was shortened to 100 μs (Figs. 1b, d) the intensity of the baseline was close to zero. Therefore, working in the microsecond range instead of the millisecond range, makes it possible to reduce the contribution of the background and thus to improve the size detection limits.

View Article Online
DOI: 10.1039/C7JA00378A

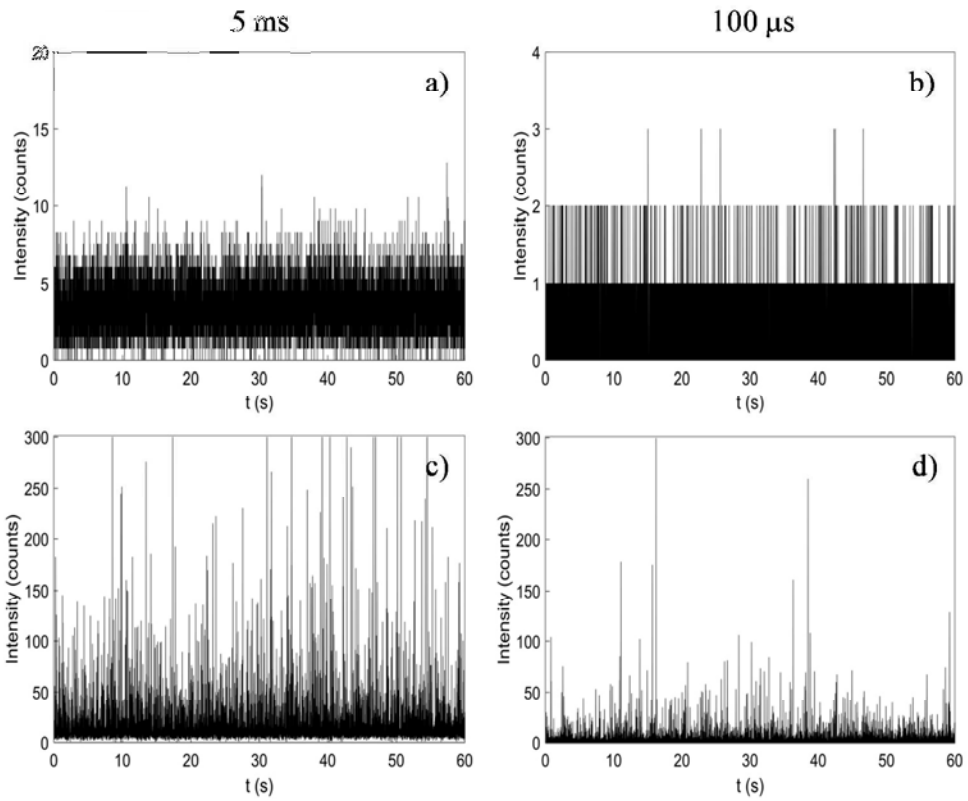

Fig. 1 ^{80}Se time scans of (a-b) ultrapure water, (c-d) 50-nm nanoparticle suspension of 1.85 x 10^8 L^{-1}. Dwell times: 5 ms, 100 µs.

3.2. Size detection limits

The intensity corresponding to the dissolved species or/and the background (μ_B) affects directly the attainable size detection limit (LOD_{size}) through its standard deviation (σ_B). Applying a 3σ criterion[25] for spherical, solid, and pure nanoparticles, and estimating σ_B as the square root of the background counts plus one[31], the LOD_{size} is given by:

View Article Online
DOI: 10.1039/C7JA00378A

$$LOD_{size} = \left(\frac{18\,\sigma_B}{\pi\,\rho\,X_{NP}K_{ICPMS}K_M}\right)^{\frac{1}{3}} = \left(\frac{18\,\sqrt{\mu_B + 1}}{\pi\,\rho\,X_{NP}K_{ICPMS}K_M}\right)^{\frac{1}{3}} \quad (1)$$

where ρ is the density of the nanoparticles, X_{NP} the mass fraction of the element in the nanoparticle, K_{ICPMS} the detection efficiency (ratio of the number of ions detected versus the number of atoms introduced into the ICP), and K_M (=AN_{Av}/M_M) includes the contribution from the element measured (A, atomic abundance of the isotope considered; N_{Av}, Avogrado number; M_M, the atomic mass).

Apart from the influence of dissolved/background on LOD_{size}, Equation 1 includes the detection efficiency, which depends on the particular instrument. On the other hand, the relationship between the signal R (ions counted per time unit) and the mass concentration C^M of a solution of an analyte nebulized into an ICPMS can be expressed as:

$$R = K_{intr}K_{ICPMS}K_M C^M \quad (2)$$

where K_{intr} (= $\eta_{neb}\,Q_{sam}$) represents the contribution from the sample introduction system, through the nebulization efficiency (η_{neb}) and the sample uptake rate (Q_{sam}), whose values are detailed in section *2. Experimental*. By analysing a dissolved selenium standard and knowing the value of K_{intr}, the term "$K_{ICPMS}\,K_M$" can be deduced from Equation 2.

Table 3 summarizes the LOD_{size} calculated for different selenium isotopes and dwell times in water. By monitoring the most abundant isotope ^{80}Se, working with H_2 as reaction gas and with a dwell time of 100 µs, a size detection limit of 18 nm could be achieved, considering: μ_B = 0.0092 counts; ρ = 4.79 g cm^{-3}; X_M = *1;* η_{neb} = 0.035; Q_{sam} = 0.35 mL min^{-1}; A = 0.4961; N_{Av} = 6.022 x

View Article Online
DOI: 10.1039/C7JA00378A

10^{23}; M_M = 78.96 g mol^{-1}; R/C^M = 40600 cps L μg^{-1}. Taking the above into account, monitoring ^{80}Se and working in collision/reaction cell mode was concluded to be the best choice for the detection of SeNPs by SP-ICPMS.

Table 3 Size detection limits for selenium nanoparticles in water, nm

Dwell time	H_2 cell	^{78}Se, LOD_{size}	^{80}Se, LOD_{size}
5 ms	No	83	-
	Yes	25	24
100 µs	No	43	-
	Yes	24	18

3.3. Analysis of commercial suspensions of selenium nanoparticles

Two different commercial suspensions of SeNPs with nominal diameters of 50 and 100 nm were analyzed by the developed method. Fig. 2 shows the time scans and the corresponding number size distribution obtained for both commercial suspensions.

View Article Online
DOI: 10.1039/C7JA00378A

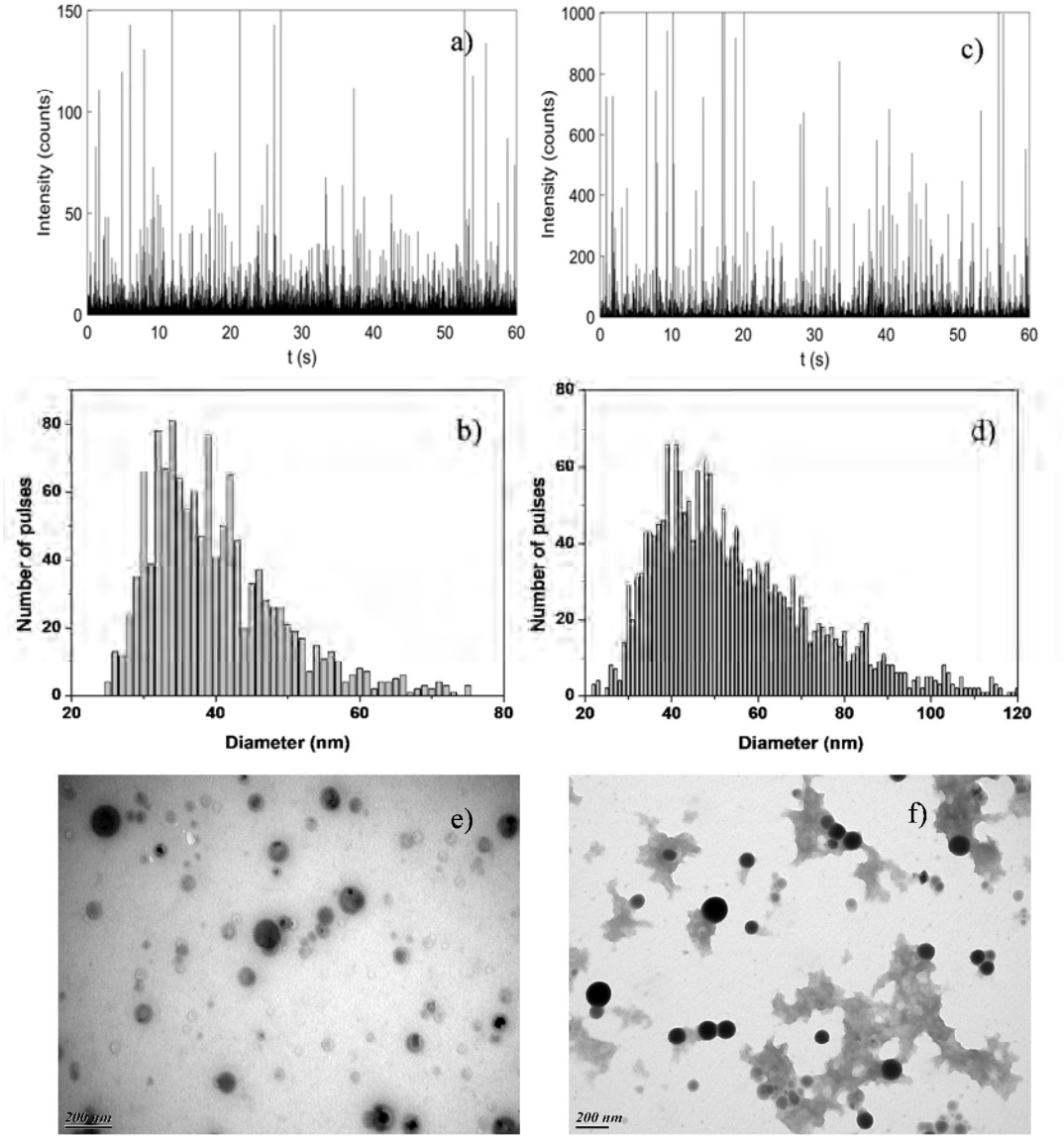

Fig. 2 ^{80}Se time scans of a) 50-nm Se nanoparticle suspension; c) 100-nm Se. Number size distribution of b) 50-nm Se nanoparticle suspension; d) 100-nm Se. Dwell time: 100 µs. Transmission electron microscope image of e) 50-nm Se nanoparticle suspension; f) 100-nm Se. Scale bar: 200 nm.

View Article Online
DOI: 10.1039/C7JA00378A

The developed method allowed the detection of SeNPs as small as 20 nm in diameter. The distributions showed an average diameter of 40.2 ± 0.4 nm for the nominal 50-nm particles and of 57.1 ± 0.1 nm for the nominal 100-nm particles. TEM images for both suspensions are presented in Fig. 2e and 2f, showing spherical particles with no significant aggregation/agglomeration and some polydispersity. The corresponding size distributions have been included in Fig. S2, showing that the average sizes are in agreement with the nominal values (60 and 101 nm, respectively).

The disagreement between TEM and SP-ICPMS results can be explained by a different response of the ICPMS towards the dissolved and the nanoparticulate selenium forms. To prove this hypothesis, the total content of selenium in the commercial suspensions of SeNPs was determined both by direct analysis of the diluted suspensions, and after their acid digestion. The calibration was achieved with aqueous standards of selenium in water and 2% HNO_3 respectively, since a dependence of the medium on the selenium sensitivity was observed. In order to verify the completeness of the digestion procedure, the corresponding digested solutions were also measured in single particle mode. No nanoparticle signals were observed, confirming that all the selenium present was in its dissolved form or as particles below 18 nm. The concentrations determined in water for the 50-nm and 100-nm SeNPs suspensions were 81.0 ± 3.4 % and 66.1 ± 7.6 % with regard to the concentration determined after acid digestion, respectively (Table 4). These results show that ICPMS sensitivity is dependent on the physicochemical form of selenium and on the size of the nanoparticles. If nebulization efficiency is considered equal for dissolved and particulated forms of selenium, the differences arises from the detection efficiency, most probably the less efficient atomization or ionization of selenium nanoparticles.

View Article Online
DOI: 10.1039/C7JA00378A

Table 4 Determination of selenium concentration in commercial suspensions of SeNPs in mg L^{-1} (mean ± standard deviation)

Sample	50-nm	100-nm
Acid digestion	148.6 ± 5.5	92.1 ± 1.20
Suspensions in water	120.3 ± 2.2	60.85 ± 6.93

The different behaviour observed for the dissolved and nanoparticulate forms of selenium implies that the use of dissolved selenium standards for calculations of the selenium mass per particle or the size of a selenium particle will produce a negative bias and hence SeNPs with similar selenium content or size of the targets should be used as standards.

3.4. Detection and characterization of biogenic selenium nanoparticles in Se-rich yeast samples

The developed method was applied for the detection and characterization of putative selenium nanoparticles present in selenium enriched yeast.

3.4.1. Enzymatic digestion of the yeast matrix. Yeast samples were submitted to an enzymatic digestion prior to their injection onto a size exclusion column for the separation of the selenium-binding species as explained in section *2. Experimental*. The effect of the digestion procedure on the stability of SeNPs (dissolution or agglomeration) was also checked. For this, a Se-free yeast sample was spiked with 100-nm SeNPs, submitted to the enzymatic digestion and analyzed by SP-ICPMS. The size distribution obtained is shown in Fig. 3. In comparison with the size distribution obtained for the original suspension (Fig. 2d), the size range was in good

View Article Online
DOI: 10.1039/C7JA00378A

agreement, proving that no agglomeration process occurred. However, obtaining the full distribution was hampered by the presence of a relatively high background level, suggesting the presence of dissolved selenium due to the partial oxidation of the nanoparticles.

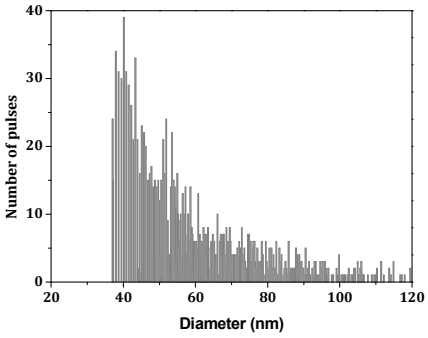

Fig. 3 Number size distribution of 100-nm SeNPs suspensions after the enzymatic procedure.

3.4.2. Detection of selenium nanoparticles in yeast. The chromatograms obtained for a Se-rich yeast sample by size exclusion chromatography with Visible and ICPMS detection are shown in Fig. 4. Low molecular weight species were eluted as a single peak at 28 minutes, whereas another selenium containing peak was observed at the exclusion volume of the column (10 min). Only the peak at the exclusion volume also showed absorption at 565 nm, a wavelength associated to SeNPs,[20,38] what suggests the presence of naturally occurring selenium nanoparticles in the yeast sample.

Furthermore, the sample of yeast after the digestion procedure (Sample A) and the collected fraction corresponding to the exclusion volume in the chromatogram (Sample A post column) were analysed by SP-ICPMS under the previously optimized conditions (monitoring ^{80}Se, with H_2

View Article Online
DOI: 10.1039/C7JA00378A

reaction cell, dwell time: 100 μs). The time scans obtained showed a significant number of signals above the background related to the presence of selenium-bearing nanoparticles in both cases (Figs. 5a, c). These time scans were transformed into signals distributions (Fig. S3). A different Se-rich yeast sample (Sample B) was submitted to the same procedure and analysed by SP-ICPMS. In this case, only a few signals above the background were observed (Fig. 5e), meaning the presence of a small amount of selenium-bearing nanoparticles. This difference may be explained by the different total concentration values in the original samples. The original yeast of sample A contained 3000 mg kg^{-1} while the total selenium concentration in the original yeast of sample B was 2000 mg kg^{-1}. On the other hand, and in order to evaluate the particle detection capabilities of the method in real samples, the size detection limits of the different samples were calculated by using the background signal obtained in the time scans, obtaining values of 23, 20 and 19 nm for Sample A, Sample A post column and Sample B, respectively.

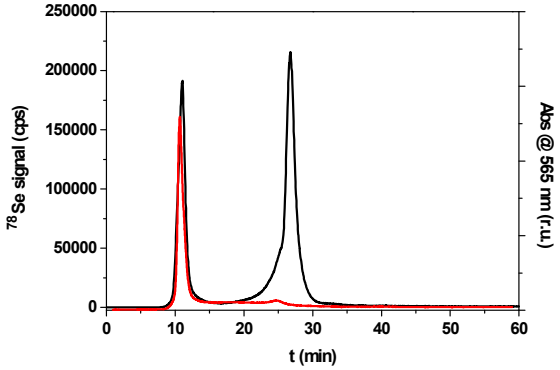

Fig. 4 Chromatograms of a selenium enriched yeast sample after the digestion procedure, obtained by ^{78}Se signal (black signal) and Vis signal recorded at 565 nm (red line). The first peak corresponds to the void volume of the column.

View Article Online
DOI: 10.1039/C7JA00378A

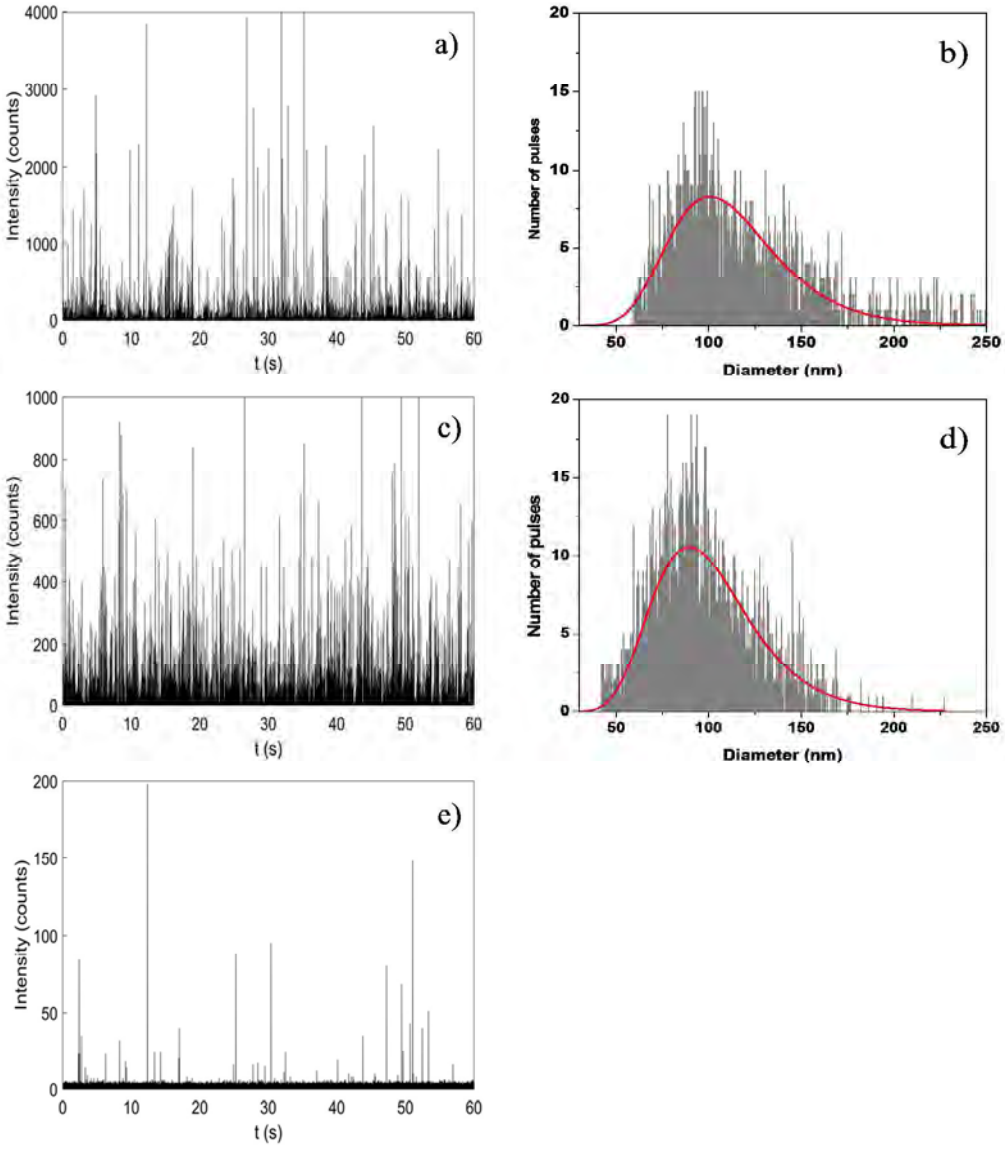

Fig. 5 ^{80}Se time scans and number size distributions obtained by SP-ICPMS corresponding to a-b) Sample A; c-d) Sample A post column; and time scan corresponding to e) Sample B.

View Article Online
DOI: 10.1039/C7JA00378A

3.4.3. Size distribution of selenium nanoparticles. SP-ICPMS provides information about the mass of element per nanoparticle, which means that the conversion into size involves knowing the actual composition, density and shape of the nanoparticles. Additional techniques like transmission electron microscopy (TEM) and energy dispersive X-ray spectroscopy (EDS) were used to learn the shape and the elemental composition of the nanoparticles present in sample A. TEM images and EDS spectra obtained confirmed the presence of spherical nanoparticles whose composition was associated to elemental selenium (Fig. S4). Note that due to the low concentration of SeNPs in the sample, the number of particles detected in the images was too low to obtain a representative histogram, although a diameter around 100 nm could be measured from single images.

Once the composition and the shape of the nanoparticles were determined, the time scans were transformed into size distributions (Figs. 5b, d), using the density of bulk elemental selenium (4.79 g cm^{-3}). Due to the different behaviour in the ICPMS with respect to the size and the physicochemical forms of selenium, as previously discussed, and to the size of nanoparticles observed by TEM (~ 100 nm), a sensitivity correction factor of 66 % was applied on the mass of selenium per nanoparticle, calculated by using aqueous standards of selenium in water. The size histogram obtained for Sample A showed a broad distribution of selenium nanoparticles, from 60 to 200 nm (Fig. 5b). The size distribution was fitted into a log normal distribution and the median diameter was calculated, obtaining an average median diameter (n=5) of 108 ± 4 nm (average ± standard deviation). On the other hand, a similar size distribution was obtained for the fraction collected at the exclusion volume of the column (Sample A post column, Fig. 5d), with an average median diameter of 97 ± 3 nm (average ± standard deviation). These results are in good agreement

View Article Online
DOI: 10.1039/C7JA00378A

with the data from TEM, where nanoparticles around 100 nm were observed and confirmed that a process of biosynthesis of selenium nanoparticles occurred in selenium enriched yeast.

4. Conclusions

An analytical method based on SP-ICPMS was developed for the detection and characterization of SeNPs. The carefully optimization of parameters, including the monitored isotope, the choice of the microsecond dwell time regime and the use of collision/reaction cell, allowed the reduction of the background signal for using the most sensitive isotope of selenium. Under the optimal conditions, a size detection limit of 18 nm could be obtained, which represents a gain of a factor of 10 in terms of the prediction made elsewhere and the first ever single particle-ICP MS method for selenium nanoparticle analysis. The method demonstrated the presence of SeNPs with sizes from 40 to 200 nm in Se-rich yeast and is able to provide information about the presence and size distributions of nanoparticles at actual concentrations.

Conflicts of interest

There are no conflicts to declare.

Supplementary Information

Electronic supplementary information (ESI) available: Information about isotopic abundance and spectral interferences for Se isotopes, time scans of ultrapure water, size distributions of SeNPs suspensions, signal distributions of samples, TEM image and EDS spectrum.

View Article Online
DOI: 10.1039/C7JA00378A

Acknowledgements

The authors acknowledge Philippe Le Coustumer and the Bordeaux Imaging Center (*BIC*) for the transmission electron microscopy and energy dispersive X-ray spectroscopy analysis. This work was supported by the Spanish Ministry of Economy and Competitiveness and the European Regional Development Fund, project CTQ2015-68094-C2-1-R (MINECO/FEDER) as well as by the project AQUITRACES Region Aquitaine 20131206001-13010973.

References

1. M. Shakibaie, H. Forootanfar, Y. Golkari, T. Mohammadi-Khorsand, and M. R. Shakibaie, *J. Trace Elem. Med. Biol.*, 2015, **29**, 235–241.
2. E. Cremonini, E. Zonaro, M. Donini, S. Lampis, M. Boaretti, S. Dusi, P. Melotti, M. M. Lleo, and G. Vallini, *Microb. Biotechnol.*, 2016, **9**, 758–771.
3. S. Lampis, E. Zonaro, C. Bertolini, P. Bernardi, C. S. Butler, and G. Vallini, *Microb. Cell Fact.*, 2014, **13**, 35.
4. S. Lampis, E. Zonaro, C. Bertolini, D. Cecconi, F. Monti, M. Micaroni, R.J. Turner, C.S. Butler, and G. Vallini, *J. Hazard. Mater.*, 2017, **324**, 3–14.
5. E. Herrero and R. Wellinger, *Microb. Cell*, 2015, **2**, 139–149.
6. G. N. Schrauzer, *Pure Appl. Chem.*, 2006, **78**, 105–109.
7. M. P. Rayman, *Br. J. Nutr.*, 2004, **92**, 557.

View Article Online
DOI: 10.1039/C7JA00378A

8. K. Bierla, J. Szpunar, A. Yiannikouris, and R. Lobinski, *TrAC - Trends Anal. Chem.*, 2012, **41**, 122–132.
9. H. Goenaga-Infante, R. Sturgeon, J. Turner, R. Hearn, M. Sargent, P. Maxwell, L. Yang, A. Barzev, Z. Pedrero, C. Cámara, V. Díaz Huerta, M. L. Fernández Sánchez, A. Sanz-Medel, K. Emese, P. Fodor, W. Wolf, R. Goldschmidt, V. Vacchina, J. Szpunar, L. Valiente, R. Huertas, G. Labarraque, C. Davis, R. Zeisler, G. Turk, E. Rizzio, L. G. MacKay, R. B. Myors, D. L. Saxby, S. Askew, W. Chao, and W. Jun, *Anal. Bioanal. Chem.*, 2008, **390**, 629–642.
10. European Food Safety Authority, *EFSA J.*, 2008, **766**, 1–42.
11. S. Mounicou, M. Dernovics, K. Bierla, and J. Szpunar, *Talanta*, 2009, **77**, 1877–1882.
12. F. A. Aborode, A. Raab, S. Foster, E. Lombi, W. Maher, E. M. Kruppa, and J. Feldmann, *Metallomics*, 2015, **7**, 1056–1066.
13. Z. Mester, *European Symposium on Atomic Spectrometry ESAS,* 2014.
14. S. Dhanjal and S. S. Cameotra, *Microb. Cell Fact.*, 2010, **9**, 52.
15. R. Avendaño, N. Chaves, P. Fuentes, E. Sánchez, J. I. Jiménez, and M. Chavarría, *Sci. Rep.*, 2016, **6**, 37155.
16. Y. Tan, R. Yao, R. Wang, D. Wang, G. Wang, and S. Zheng, *Microb. Cell Fact.*, 2016, **15**, 157.
17. A. V. Tugarova, E. P. Vetchinkina, E. A. Loshchinina, A. M. Burov, V. E. Nikitina, and A. A. Kamnev, *Microb. Ecol.*, 2014, **68**, 495–503.
18. A. A. Kamnev, P. V. Mamchenkova, Y. A. Dyatlova, and A. V. Tugarova, *J. Mol. Struct.*, 2017, **1140**, 106–112.
19. F. Elahian, S. Reiisi, A. Shahidi, and S. A. Mirzaei, *Nanomedicine Nanotechnology, Biol. Med.*, 2017, **13**, 853–861.

View Article Online
DOI: 10.1039/C7JA00378A

20. S. Dwivedi, A. A. AlKhedhairy, M. Ahamed, and J. Musarrat, *PLoS One*, 2013, **8**, 1–10.

21. M. Palomo-Siguero, P. Vera, Y. Echegoyen, C. Nerin, C. Cámara and Y. Madrid, *Spectrochim. Acta Part B J.*, 2017, **132**, 19–25.

22. G. Moreno-Martin, M. Pescuma, T. Pérez-Corona, F. Mozzi and Y. Madrid, *Anal. Chim. Acta*, 2017, **992**, 34–41.

23. F. Laborda, E. Bolea, and J. Jiménez-Lamana, *Trends Environ. Anal. Chem.*, 2016, **9**, 15–23.

24. C. Degueldre and P. Y. Favarger, *Colloids Surfaces A Physicochem. Eng. Asp.*, 2003, **217**, 137–142.

25. F. Laborda, E. Bolea, and J. Jiménez-Lamana, *Anal. Chem.*, 2014, **86**, 2270–2278.

26. F. Laborda, J. Jiménez-Lamana, E. Bolea, and J. R. Castillo, *J. Anal. At. Spectrom.*, 2011, **26**, 1362.

27. S. Lee, X. Bi, R. B. Reed, J. F. Ranville, P. Herckes, and P. Westerhoff, *Environ. Sci. Technol.*, 2014, **48**, 10291–10300.

28. J. Goossens, L. Moens, and R. Dams, *Talanta*, 1994, **41**, 187–93.

29. S. D. Tanner, V. I. Baranov, and D. R. Bandura, *Spectrochim. Acta - Part B At. Spectrosc.*, 2002, **57**, 1361–1452.

30. H. E. Pace, N. J. Rogers, C. Jarolimek, V. A. Coleman, C. P. Higgins, and J. F. Ranville, *Anal. Chem.*, 2012, **84**, 4633.

31. F. Laborda, J. Jiménez-Lamana, E. Bolea, and J. R. Castillo, *J. Anal. At. Spectrom.*, 2013, **28**, 1220–1232.

32. I. Feldmann, N. Jakubowski, C. Thomas, and D. Stuewer, *Fresenius. J. Anal. Chem.*, 1999, **365**, 422–428.

View Article Online
DOI: 10.1039/C7JA00378A

33. J. M. Marchante-Gayon, C. Thomas, I. Feldmann, and N. Jakubowski, *J. Anal. At. Spectrom.*, 2000, **15**, 1093–1102.

34. I. Abad-Álvaro, E. Peña-Vázquez, E. Bolea, P. Bermejo-Barrera, J. R. Castillo, and F. Laborda, *Anal. Bioanal. Chem.*, 2016, **408**, 5089–5097.

35. J. J. Sloth and E. H. Larsen, *J. Anal. At. Spectrom.*, 2000, **15**, 669–672.

36. U. Völkopf, K. Klemm, and M. Pfluger, *At. Spectrosc.*, 1999, **20**, 53–59.

37. S. D. Tanner, V. I. Baranov, and U. Vollkopf, *J. Am. Soc. Mass Spectrom.*, 2000, **15**, 1261–1269.

38. Z. H. Lin and C. R. C. Wang, *Mater. Chem. Phys.*, 2005, **92**, 591–594.